065 **COMPARISON BETWEEN CRAWLING WAVE SONOELASTOGRAPHY AND STL-ARFI IN BIOMATERIALS.**

Juvenal Ormachea[1], Arthur Salo[2], Amy Lerner[2], Steve McAleavey[2], Benjamin Castaneda[1]*
[1]Pontificia Universidad Católica del Perú, Av. Universitaria 1801, San Miguel, Lima, Lima, PERU;
[2]University of Rochester, 252 Elmwood Ave., Rochester, NY, 14627, USA.

Submitted for publication in final form: October 1, 2013.

Introduction

In the last five years, various groups have performed comparative studies between different elastographic techniques in order to make a better characterization for biomaterials [1] or human tissue [2], to understand what elastic modulus is measured [3] and the factors that influence their precision and accuracy [4]. These comparisons evaluated the shear wave speed generated in the medium, the shear modulus or the Young's modulus. Some of these comparisons validated their work using mechanical testing to evaluate elastic properties, or a rheometer to measure the linear viscoelasticity in the materials [1]. Another work compares the spatial resolution, the contrast and the contrast to noise ratio (CNR) and evaluated the advantages and disadvantages of each technique (Acoustic radiation force impulse and shear wave elastography imaging) [5]. It is worth mentioning that, many studies evaluated how one of the elastographic techniques is complementary with the other. For example, in [1], they use transient elastography (TE) and supersonic shear imaging (SSI) to obtain a better characterization using a wide range of frequencies, another work use acoustic radiation force impulse (ARFI) and shear wave elastography (SWE) to image the structures in the material because they found that SWE has better contrast and CNR but lower spatial resolution than ARFI [5].

Following this line of studies, we present a comparison between two elastographic techniques: Crawling Wave Sonoelastography (CWS) and Single Tracking Location-Acoustic Radiation Force Impulse (STL-ARFI). In CWS, an elasticity imaging technique proposed by Wu *et al.* [6], two opposing shear wave vibration sources are operated at slightly offset frequencies and produce a slowly moving interference pattern, termed crawling waves, which is imaged in real time using vibration sonoelastography. This technique offers a quantitative estimation of the elastic properties of the tissue. CWS has been successfully applied to detect radio frequency ablated hepatic lesions *in vitro* [7], to characterize human skeletal muscle *in vivo* [8, 9] and to characterize human prostate tissue *ex vivo* [10]. STL-ARFI estimates the shear wave speed generated from an acoustic radiation force (ARF) [11]. In this method, a single tracking location is required for measuring the tissue displacement. STL-ARFI has the advantage to be less sensitive to speckle-induced phase errors since the measurement is differential in nature and cancels out this source of error [11]. This technique has been applied in phantoms and excised porcine liver tissue [11, 12].

CWS and STL-ARFI are quantitative elastographic techniques that estimate the SWS. Both techniques have been validated independently in phantoms and soft tissues. However there is a lack of comparison between these techniques in the literature. In this paper, we present a comparison between CWS and STL-ARFI in the estimation of the shear wave speed in phantoms.

Materials and methods

In this chapter we describe the experiments using homogeneous phantoms. To perform the comparison, the shear wave speed was assessed for each technique. Furthermore, mechanical tests were applied to confirm the validity of the results. All the experiments were performed at room temperature (20-21^{o}C) and at the same day to avoid changes in the materials. The mechanical testing and ultrasound scans were made in three different laboratories at University of Rochester.

A. Homogeneous phantoms

Homogeneous elastic and viscoelastic phantoms were made following the procedure by Hah et al [13]. Two different phantoms, 10% and 16% gelatin (300 Bloom Pork Gelatin, Gelatin Innovations Inc.), were created by heating a mixture of gelatin, 1.8L degassed water, 16.2g NaCl, 36g of graphite and 2.7g agar to 50^{o}C. The mixture was then cooled to approximately 30^{o}C and poured into the cubic mold. The mold was then allowed to rest at 4^{o}C overnight. In addition, an oil-based gelatin phantom (viscoelastic phantom) was created. It consisted of 10% gelatin and 15% castor oil, 26g of graphite and 1L of degassed water. The

mixture was heated to 70°C. After that, the molten gelatin was cooled to around 55°C. Then, 325mL castor oil and 10mL surfactant (Ultra Ivory, Procter & Gamble, Cincinnati, OH, USA) were emulsified into the mixture. The mixture was cooled to approximately 30°C, poured in a cubic mold and allowed to rest at 4°C overnight.

B. Mechanical measurements (MM)

Stress relaxation tests were performed on three cylindrical samples (approximately 38.08 mm in diameter and 33 mm in length). The samples were made with the same mixture used to create the homogeneous phantom previously. The mechanical tests were applied using the procedure described by Zhang et al [14]. A QT/5 mechanical device (MTS Systems Co., Eden Prairie, MN, USA) with a 5 N load cell was used to test the samples. The upper and lower plates were coated with vegetable oil before testing. The samples were put on the center of the lower testing plate. The top plate was used as a compressor and carefully positioned to fully press the sample. The compression rate and the strain value were adjusted to 0.5 mm/s and 5%, respectively. The tests lasted about 700 s. The resulting data consisted of a plot of the stress versus time. The stress relaxation curve of each sample was fitted to the Kelvin Voigt Fractional Derivative (KVFD) model using the MATLAB Curve Fitting Toolbox. The trust-region method for nonlinear least squares fitting was applied on each curve. Then, the elasticity modulus at any frequency was determined using equation 1.

$$E(f) = E_o + \eta \cos\left(\frac{\pi\alpha}{2}\right)(2\pi f)^{\alpha} \ , \tag{1}$$

where $E(f)$ is the elasticity modulus at any frequency, f the frequency, E_o the relaxed elastic constant, η the viscoelastic parameter and α the order of the fractional derivative.

In order to obtain a relationship between the shear wave speed and the elasticity modulus, it is assumed that phantoms are nearly incompressible, and, therefore, their Poisson's ratio (ν) is approximately 0.5. Finally, we use equation 2 to estimate the shear wave speed:

$$c_s(f) \approx \sqrt{\frac{E(f)}{3\rho}} \ , \tag{2}$$

where $c_S(f)$ is the shear wave speed at any frequency and ρ the density of material that is assumed to be 1g/cm^3. Mechanical measurements were considered as ground truth.

C. Crawling wave sonoelastography

An amplifier (model 5530, AE Techron, Elkhart, IN, USA) driven by a dual channel function generator (model AFG3022B, Tektronix, Beaverton, OR, USA) provided input signals to two mechanical vibration sources (Brüel & Kjaer, Naerum, Denmark) vibrating at low frequencies (140-360Hz) and applied on the homogeneous phantoms to generate a relatively uniform vibration field. A GE Logiq 9 ultrasound system (GE Ultrasound, Milwaukee, WI) was used to perform sonoelastographic imaging and a linear array ultrasound transducer (M12L, GE Healthcare, Milwaukee, WI, USA) was positioned between the vibration sources. To estimate the shear wave speed, the phase of the crawling wave signal was extracted using the method described in [13] and equation 3.

$$c_s(f) = \frac{2\pi f_v}{\theta'(x)}, \tag{3}$$

where f_v is the vibration frequency and $\theta(x)$ the unwrapped phase of the crawling wave signal. We obtained the phase by taking the Fourier transform of each pixel projection of the crawling wave image over the time axis.

D. Single tracking location acoustic radiation force

A Siemens Antares scanner (Siemens Medical Solutions, USA,) and a linear array transducer, a Siemens Antares VF7-3 linear array, were used to generate the pushing beams as well as to track the induced displacements. The center frequency of both the push and track pulses was 4.21 MHz. In the STL-ARFI algorithm, the acoustic radiation force was applied at two locations, P_1 and P_2, 2.1 mm apart, and the

induced shear waves were tracked at one location, T, 1.8 mm from P_1. The shear modulus estimate is associated with the region between the two pushing pulses. The post-push tracking echoes were received at a pulse repetition frequency of 7.5 kHz. The displacements were estimated using normalized cross-correlation on the reference and post-push echoes. The finite-time difference of the slow-time displacement was calculated to get the velocity data. The velocity data associated with the two pushes were cross-correlated to extract the arrival time difference between both waves. After that, the shear wave speed was estimated using:

$$C_s = \frac{\Delta x}{\Delta t}, \tag{4}$$

Where Δx is the distance between P_1 and P_2, Δt is the arrival time difference. Then, the power spectral density (PSD) was used to estimate the frequency range of the velocity signal generated by the acoustic radiation force in P_1 and P_2.

Finally, in order to compare the estimations of CWS and STL-ARFI, a linear fit was applied to extrapolate the values obtained by CWS [15]. These values were compared with those that we obtained with MM method.

Results

Figure 1 shows a typical stress relaxation curve of a sample and its fit using the KVFD model. Each curve fitting had a correlation coefficient value larger than 0.93, demonstrating that the KVFD model is useful for this purpose. As we explained previously, the PSD of the velocity signal from STL-ARFI was estimated in order to obtain its frequency range. We found a frequency range of 400-1500Hz. For the comparison purpose, we chose the value of 500Hz because it was the peak value in many cases (Figure 2)

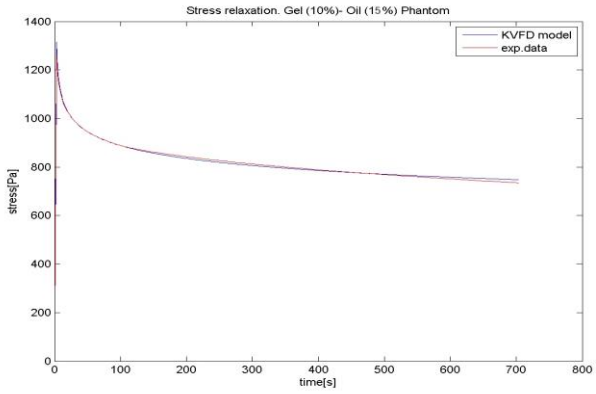

Figure 1. Stress relaxation curve (red line) and its fitting using the KVFD model (blue line).

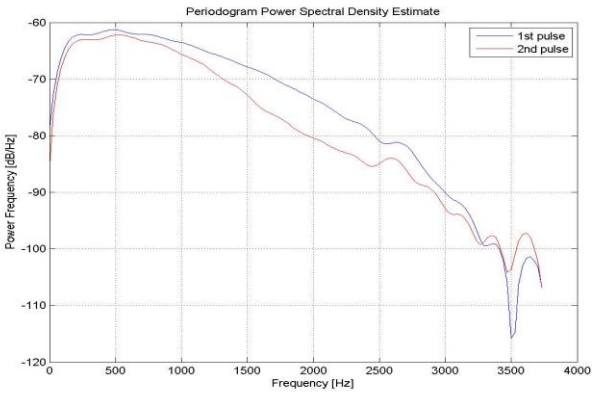

Figure 2. Power Spectral Density estimation of the velocity signals generated by P_1 (blue) and P_2 (red)

Figure 3.a shows two shear waves maps estimated with CWS (left image) and STL-ARFI (right image). Subsequently, a region of interest (1.5x1.0xm) was extracted from the center of each image to obtain the shear wave speed average and its standard deviation. Figure 3.b, 3.c and 3.d shows the comparison plots (shear wave speed vs. frequency) obtained by CWS, STL-ARFI and mechanical measurements in the region of interest from the 10%, 16% and oil-based phantom respectively. The shear wave speed at 500Hz, estimated by CWS (extrapolate value), STL-ARFI and mechanical measurements respectively, were 4.04m/s, 4.06±0.05m/s and 4.29±0.72m/s (10% phantom); 5.07m/s, 5.54±0.69m/s and 5.09±0.79m/s (16% phantom) and 4.48m/s, 5.09±0.23m/s and 4.51±0.70m/s (oil-based phantom). Furthermore, the maximum standard deviation for CWS for its frequency range (140-360Hz) were 0.43m/s, 0.05m/s and 0.72m/s from 10%,16% and oil-based phantom respectively. Due to mechanical measurements were considered as ground truth, the estimated error of the shear wave speed value at 500Hz from CWS were 0.26m/s, 0.69m/s and 0.22m/s; from STL-ARFI were 0.13m/s, 0.88m/s and 0.58m/s (10%, 16% and oil-based phantom respectively).

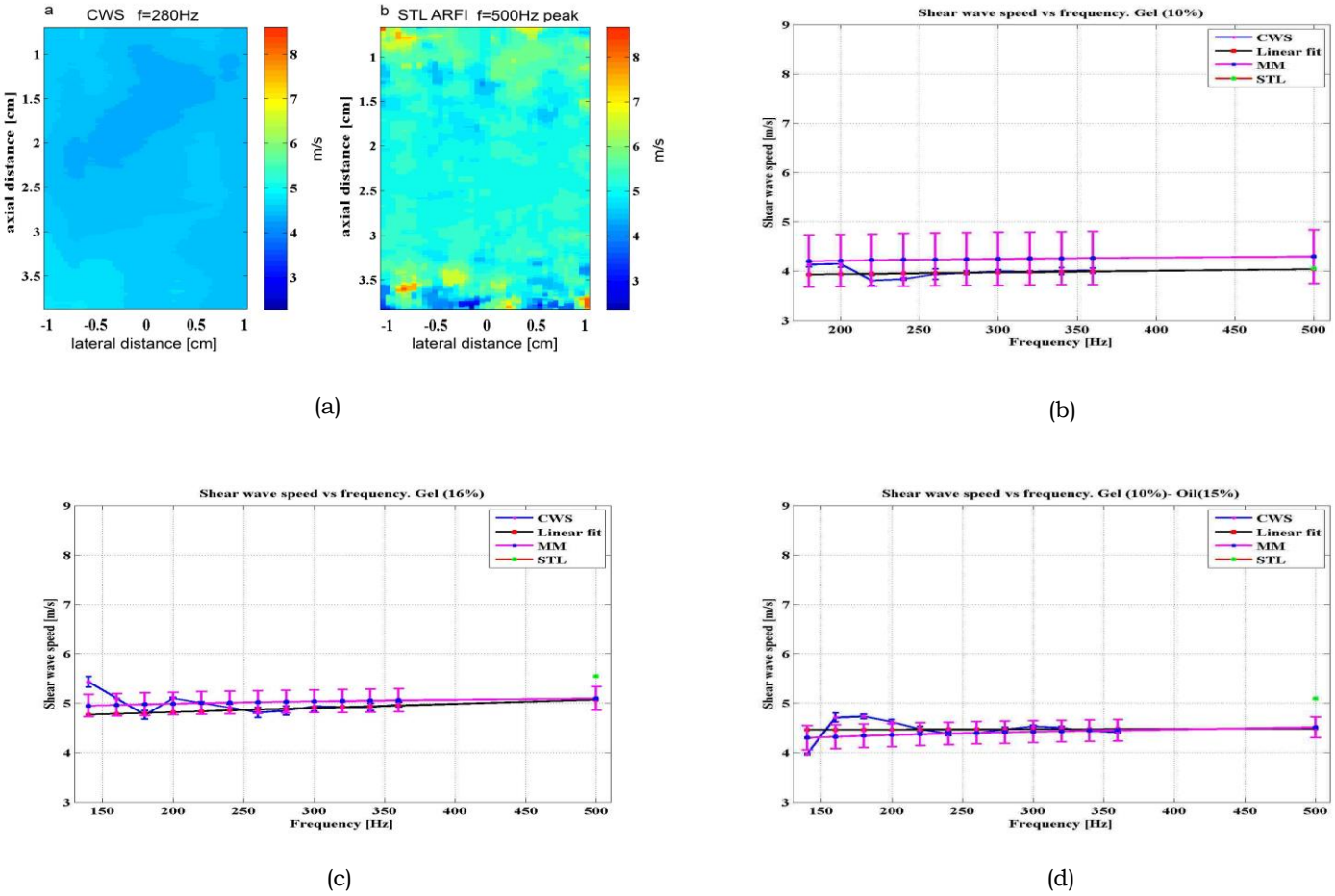

Figure 3. (a) Shear wave speed maps estimated with CWS (left) and STL-ARFI (right) for a 16% phantom, (b) comparison plot of CWS, STL-ARFI, MM in a pure 10%, (c) 16% gelatin phantom and (d), an oil-based (gel 10% oil 15%) phantom. The linear fitting was done in order to extend the CWS-SWS values to 500Hz

Discussion and conclusions

In this study, only elastic and viscoelastic phantoms were evaluated by both elastographic techniques and mechanical measurements. For the three different homogenous phantoms (10%, 16% gelatin and the oil-based), CWS and STL-ARFI have good agreement with the mechanical measurements (maximum error equal to 0.88m/s). In the case of elastic (16% gelatin) and oil-based phantom, STL-ARFI has a slight overestimation. This might be explained because the shear wave speed shown at 500Hz belongs to its entire range of frequencies. However, the value obtained with STL-ARFI is still very consistent with those obtained with the extension value of CWS and MM.

The correspondence between CWS and MM is better in higher frequencies (240-360Hz) because the spatial resolution improves. However, we also increase the attenuation and decrease the capacity of penetration. In lower range of frequencies (150-200Hz), CWS generate some border reflections and that could explain the differences between the shear wave speed values obtained by CWS and MM at this frequency range. Moreover, one of the advantages using CWS is its capacity of assessing the dispersion or frequency dependence of shear wave propagations.

CWS and STL-ARFI operate at different frequencies range, this is important for a better characterization of materials. Moreover, the shear wave speed values obtained with CWS and STL-ARFI seems to be quite similar to those reported in the literature from tissue mimicking phantoms (2m/s - 6.5m/s) [1-5]. Furthermore, the results of this study contribute to the limited data currently available for comparison elastographic techniques and generate more support in the application of elastography.

In the case of the oil-based phantom, we expected to get a higher slope compared to pure elastic phantoms. However, the slope is similar to those obtained with the 10% and 16% gelatin phantoms. Subsequently, new work should consider add other material that could increase the viscosity properties in the phantom.

Future studies should consider a comparison of other metrics using inhomogeneous phantoms (i.e. CNR, spatial resolution) and a validation in patients in clinical settings. Additionally, since attenuation could provide another parameter with high diagnostic value, shear wave attenuation quantification by using STL-ARFI or CWS will be performed.

Acknowledgements: This project was supported by Marco Polo Award from PUCP. The authors would like to thank Kevin Parker, Ph.D. for his help and technical support.

References:

[1]. Gennisson, J. L., Marcelan, A., Dizeux, A., & Tanter, M. (2012, October). High frequency rheology of hybrid hydrogels using ultrasound transient elastography. In *Ultrasonics Symposium (IUS), 2012 IEEE International* (pp. 2525-2528). IEEE.

[2]. Song, P., Urban, M. W., Manduca, A., Zhao, H., Greenleaf, J. F., & Chen, S. (2012, October). Comb-push ultrasound shear elastography (CUSE): A novel and fast technique for shear elasticity imaging. In *Ultrasonics Symposium (IUS), 2012 IEEE International* (pp. 1842-1845). IEEE.

[3]. Xie, H., Shamdasani, V., Zhao, H., Song, P., Zhou, S., Robert, J. L., ... & Chen, S. (2012, October). A phantom study to cross-validate multimodality shear wave elastography techniques. In *Ultrasonics Symposium (IUS), 2012 IEEE International* (pp. 1858-1861). IEEE.

[4]. Maeva, A., Lee, M., & Foster, S. (2012, October). Shear wave imaging at high frequencies: A feasibility study in tissue mimicking gelatin phantoms. In *Ultrasonics Symposium (IUS), 2012 IEEE International* (pp. 2552-2554). IEEE.

[5]. Rosenzweig, S., Palmeri, M., Rouze, N., Lipman, S., Kulbacki, E., Madden, J., ... & Nightingale, K. (2012, October). Comparison of concurrently acquired in vivo 3D ARFI and SWEI images of the prostate. In *Ultrasonics Symposium (IUS), 2012 IEEE International* (pp. 97-100). IEEE.

[6]. Wu, Z., Taylor, L. S., Rubens, D. J., & Parker, K. J. (2004). Sonoelastographic imaging of interference patterns for estimation of the shear velocity of homogeneous biomaterials. *Physics in medicine and biology*, *49*(6), 911.

[7]. Hoyt, K., Castaneda, B., & Parker, K. J. (2008). Two-dimensional sonoelastographic shear velocity imaging. *Ultrasound in medicine & biology*, *34*(2), 276-288.

[8]. Hoyt, K., Castaneda, B., & Parker, K. J. (2007, October). 5C-6 Muscle Tissue Characterization Using Quantitative Sonoelastography: Preliminary Results. In *Ultrasonics Symposium, 2007. IEEE* (pp. 365-368). IEEE.

[9]. Hoyt, K., Kneezel, T., Castaneda, B., & Parker, K. J. (2008). Quantitative sonoelastography for the in vivo assessment of skeletal muscle viscoelasticity. *Physics in medicine and biology*, *53*(15), 4063.

[10]. Castaneda, B. (2009). Extracting information from sonoelastographic images. *Diss. University of Rochester*.

[11]. Elegbe, E. C., & McAleavey, S. A. (2013). Single Tracking Location Methods Suppress Speckle Noise in Shear Wave Velocity Estimation. *Ultrasonic imaging*, *35*(2), 109-125.

[12]. McAleavey, S., Collins, E., Kelly, J., Elegbe, E., & Menon, M. (2009). Validation of SMURF estimation of shear modulus in hydrogels. *Ultrasonic imaging*, *31*(2), 131-150.

[13]. Hah, Z., Hazard, C., Mills, B., Barry, C., Rubens, D., & Parker, K. (2012). Integration of crawling waves in an ultrasound imaging system. Part 2: signal processing and applications. *Ultrasound in medicine & biology*, *38*(2), 312-323.

[14]. Zhang, M., Castaneda, B., Wu, Z., Nigwekar, P., Joseph, J. V., Rubens, D. J., & Parker, K. J. (2007). Congruence of imaging estimators and mechanical measurements of viscoelastic properties of soft tissues. *Ultrasound in medicine & biology*, *33*(10), 1617-1631.

[15]. Barry, C. T., Mills, B., Hah, Z., Mooney, R. A., Ryan, C. K., Rubens, D. J., & Parker, K. J. (2012). Shear wave dispersion measures liver steatosis. *Ultrasound in medicine & biology*, *38*(2), 175-182.